Journal of Alloys and Compounds 509 (2011) 4910–4915

Contents lists available at ScienceDirect

Journal of Alloys and Compounds

journal homepage: www.elsevier.com/locate/jallcom

Thermal stability of electrical properties of ZnO:Al films deposited by room temperature magnetron sputtering

Tao Wang, Xungang Diao *, Peng Ding

School of Physics and Nuclear Energy Engineering, Beihang University, Beijing 100191, China

ARTICLE INFO

Article history:
Received 9 October 2010
Received in revised form 28 January 2011
Accepted 31 January 2011
Available online 22 February 2011

Keywords:
AZO film
Magnetron sputtering
Thermal stability
Real-time sheet resistance

ABSTRACT

In order to investigate the thermal stability of electrical properties for aluminum doped zinc oxide (ZnO:Al, AZO) films deposited by direct current reactive magnetron sputtering, AZO films deposited from an alloy target (0.8 wt.% Al) on soda-lime glasses were annealed in argon gas at different temperatures. A data capturer was applied to monitor and collect real-time sheet resistance (R_s) of the films throughout the annealing. Results revealed that R_s of the film heated at 100 °C was reduced throughout the annealing, however, conductivity of the films annealed over 100 °C was improved at early stage but then deteriorated all along to the end. Some novel R_s change points which need more penetrations were detected. The experimental results obtained from electron diffraction spectrum, X-ray diffraction pattern, X-ray photoelectron spectrum, and Hall measurement were analyzed to explore the effect of the annealing on the electrical properties of AZO films. It was found that the exotic element, which might influence the film properties, was not observed. It was also suggested that the transformation of the crystalline structure and surface chemical bonding states, which resulted in the decrease of carrier concentration and mobility could be the reason for the conductivity degeneration of the films annealed at higher temperature.

© 2011 Elsevier B.V. All rights reserved.

1. Introduction

As a direct band gap semiconductor, ZnO has band energy of more than 3.3 eV and more than 60 meV of exciton binding energy [1–4]. Because of its tremendous application potentials, various forms of ZnO such as powder [5,6], flake [7,8], film [9,10], nanorod [11], nanowire [12] and so on, have been extensively investigated. For ZnO films doped with aluminum, excellent properties such as great reflectance in infrared region, sound absorbance of UV light, more than 85% of transmittance in visible light region and specific resistivity of $1–5 \times 10^{-4}\,\Omega\,\text{cm}$ have been obtained up to now [13]. Along with other advantages like cost effectiveness, nontoxicity and high stability in hydrogen plasma, AZO film has developed to be one of the most promising substitutes for the presently predominant indium tin oxide (ITO) film in various fields, such as solar cells, light emitting diodes, laser diodes and flat display panels, etc. [14,15]. By far, extensive investigations have been focused on the fabrication process and initial qualities of AZO. In fact, secondary qualities after deposition, especially the thermal stability and weatherability of electrical properties are likewise decisive for the ultimate prospect of AZO. Hence, several literatures regarding the characteristics of AZO under post-deposition thermal treatment (at different temperatures or under varied ambient) can also be accessed. However, probably due to the limited information obtained from intermittent manual data acquisition, results from different authors often do not agree well with each other. Generally, it is believed that resistivity of AZO could be substantially increased by oxygen exposed annealing because of the decrease of oxygen vacancies which commonly serve as carrier donors [16–18]. It has also reported that the film conductivity can be improved or at least not deteriorated by carefully designed thermal treatment under oxygen deficient ambient owing to the defects removal and enhanced crystallinity [19–21]. Contrarily, some researchers have reported certain extent of conductivity degeneration after annealing without oxygen [22–24], and even remarkable conductivity improvement under oxygen annealing has been observed by Ch et al. [25]. Therefore, further investigations to disclose the whole story of the thermal stability of electrical properties for AZO film are indispensable.

In this paper, AZO films obtained from room temperature D.C. reactive magnetron sputtering were annealed in argon gas at different temperatures for more than 5 h. Throughout the annealing, an on-line data capturer was applied to monitor and collect the real-time R_s transformations of the films. Crystalline structure, sur-

* Corresponding author. Tel.: +86 10 82338779; fax: +86 10 82338779.
E-mail addresses: wang.tao_1981@163.com (T. Wang), diaoxg@buaa.edu.cn (X. Diao).

0925-8388/$ – see front matter © 2011 Elsevier B.V. All rights reserved.
doi:10.1016/j.jallcom.2011.01.210

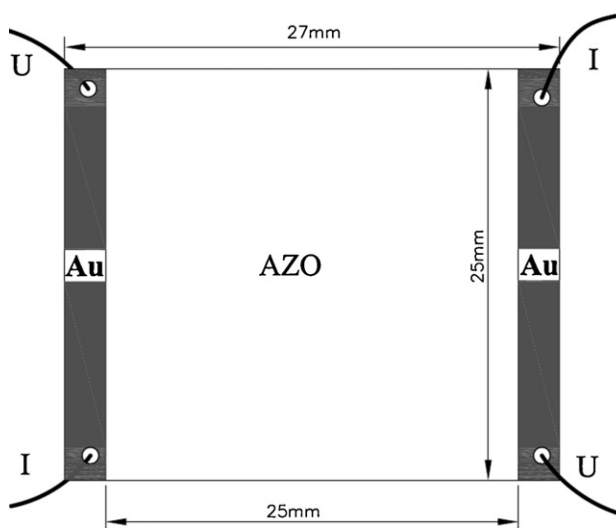

Fig. 1. Schematic configuration for the film resistance measurements.

face morphology and chemical bonding states of the films were investigated in detail before and after the annealing.

2. Experimental

A self-made magnetron sputtering system was employed in the experiment. A 6 mm thick alloy target (99.99% purity) with 60 mm in diameter was used as the sputtering source. Based on our early optimized experimental results, the doping amount of Al in the target was 0.8 wt.%. The target was fixed in a water cooling copper back plate, 6 mm away from the substrate. Substrates used are ordinary soda lime glasses with dimensions of 27 mm × 25 mm × 1 mm. All substrates were ultrasonically rinsed sequentially in acetone, ethanol, and deionized water for 10 min, respectively. When the chamber was pumped down to 1×10^{-3} Pa, sputtering gas regulated by isolated mass flow controllers was introduced in. Optimized by our previous work, partial pressure of argon and oxygen gas was fixed at 0.9 Pa, 0.1 Pa, respectively. Prior to the film deposition, 5 min of pre-sputtering was performed to clear the target surface. The sputtering power was 100 W, and there was no intentional heating during the 20 min of sputtering.

After deposition, films were annealed at varied temperatures (from 100 °C to 400 °C) in argon ambient (99.999% purity) for more than 5 h in a horizontal tube furnace. All the target temperatures were reached at a speed of 10 °C/min from 20 °C. All along the annealing, a self-designed data capturer connected to a computer was employed to record the real-time R_s of the films, with the writing interval of 1point per second. A constant current power source was employed to supply a precise current I of 1 ± 0.01 mA to intrigue the voltage U required for the R_s ($R_s = U/I$) calculations. Based on the definition of sheet resistance, the films were well connected (with 200 nm thick thermal evaporated Au film as electrodes) to the capturer in the form as displayed in Fig. 1, which is 4.53 times more sensitive to the R_s variation than conventional four point probe method.

Transmittance of the films in 300–900 nm was measured by HITACHI U-3010 UV–vis spectrophotometer. The films' thickness, crystalline structure, surface morphology, elementary composition and chemical bonding states were characterized by Dektak IIA α-step surface profiler, X-ray diffractometer (XRD) with Cu Kα_1 source, XL30 SFEG scanning electron microscope (SEM), electron diffraction spectrum (EDS), X-ray photoelectron spectrum (XPS), respectively.

3. Results and discussion

3.1. Electrical and optical properties

The thickness and original R_s of all films prepared at identical conditions are about 500 nm and lower than 50 Ω/square (hall mobility is 5.53 cm^2/V s, carrier concentration is 4.85×10^{20} cm^{-3}), respectively. As displayed in Fig. 2, R_s of the sample films are significantly dependent on both the temperature and time. At 100 °C, the R_s mildly decreases with the time during the whole process. At the early stage of 150 °C and 200 °C annealing, noticeable conductivity improvements are observed for both samples, however, as time increases further, unexpected increase of R_s is revealed. When temperature is over 200 °C, as shown, the early improving then degenerating patterns for the film conductivity are again routinely disclosed. Moreover, it is found that the ultimate conductivity deterioration can be severely enhanced when temperature was further elevated. After annealing at 400 °C, the final R_s of the film can reach more than 1500 Ω/square, the hall mobility and carrier concentration have been severely reduced to 1.17 cm^2/V s and 6.54×10^{19} cm^{-3}, respectively. Actually, all these annealing processes have been repeated several times; a copper film, indium tin oxide film connected to the capturer with the same configurations mentioned in Section 2, and an AZO film not linked to the capturer have been also annealed at 400 °C. All results have confirmed that the electrical conductivity degeneration of AZO films is not the impact imposed by the capture system but the characteristics of AZO itself. Intensive discussions on these characteristics will be given in the following. Additionally, with the advantage of non-stop data capturing, some novel inflexion points haven't covered elsewhere have been captured when temperature was over 300 °C. These turning points, which definitely might originate from certain micro-transformations are empirically defined as some possible phase transition points here. More accurate reason for these inflexion points are still not clear yet, further investigations are needed and have already been launched by us.

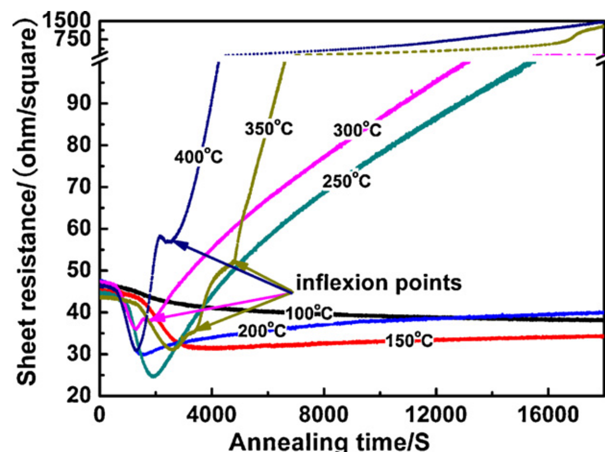

Fig. 2. Dependences of AZO films' R_s on annealing time at different temperatures.

From Fig. 3, due to the decreasing absorbance from the diminished charge carriers, and the improved crystallinity discussed in the following section, we can see the film's average transmittance (more than 80%) in the visible region (400–800 nm) is slightly

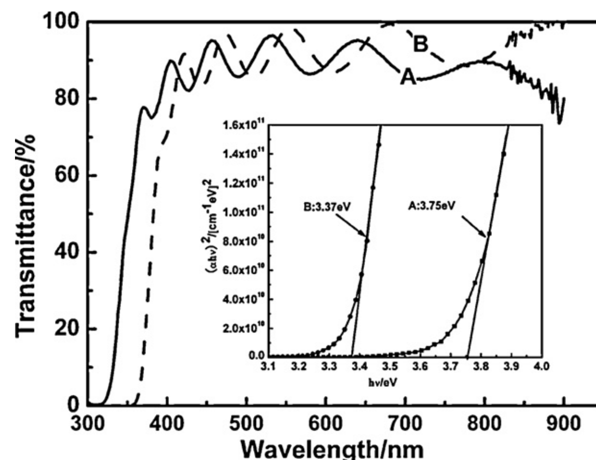

Fig. 3. Optical transmittance of AZO films before and after annealing at 400 °C. Inset: plots of $(\alpha h\nu)^2$ versus $h\nu$ and the deduced E_g of AZO films before and after annealing at 400 °C.

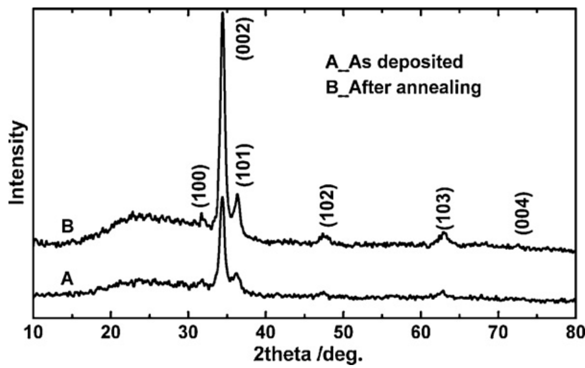

Fig. 4. X-ray diffraction patterns of AZO films before and after annealing at 400 °C.

improved after annealing at 400 °C. As a direct band gap semiconductor, the optical energy gap (E_g) of AZO film can be obtained by [24]:

$$(\alpha h\nu)^2 = C(h\nu - E_g) \quad (1)$$

where α is the optical absorption coefficient, ν is the frequency, h is the Planck constant, and C is a constant for a direct transition. Eventually, by plotting $(\alpha h\nu)^2$ versus $h\nu$ and extrapolating the linear portion of the plots to the energy axis, the E_g of the films was obtained and displayed in the inset of Fig. 3. As can be seen, the band gap of AZO film remarkably decreases from 3.75 eV to 3.37 eV after annealing at 400 °C, which is well coherent to the reduction of electrical carriers mentioned above and has been confirmed by Yang et al. [24] as well.

3.2. Microstructure and surface morphology

As shown in Fig. 4, the as-deposited AZO film has a typical c-axis (0 0 2) preferred orientation, which corresponds to a hexagonal wurtzite structure. After annealing at 400 °C, the intensified (0 0 2) peak implies that the crystallinity of the c-axis oriented grains has been improved and the grain size has been enlarged. As (0 0 2) textured AZO films have been proved to be superior in terms of electrical conductivity [26–28], the enlarged (0 0 2) oriented grains along with the release of residual stress which are labeled as positive factors here can account for the early decrease of R_s in Fig. 2. Since the as-deposited and 400 °C annealed films are both dominated by (0 0 2) preferred orientation, the corresponding grain size D could be estimated from the (0 0 2) peak by the Scherrer's formula:

$$D = \frac{0.9\lambda}{\beta \ \mathrm{Cos}\theta} \quad (2)$$

where λ (1.5405 Å) is the X-ray wavelength, β is the full width at half maximum (FWHM) of (0 0 2) peak corrected from instrumental error, and θ is the diffraction angle. The calculated grain sizes

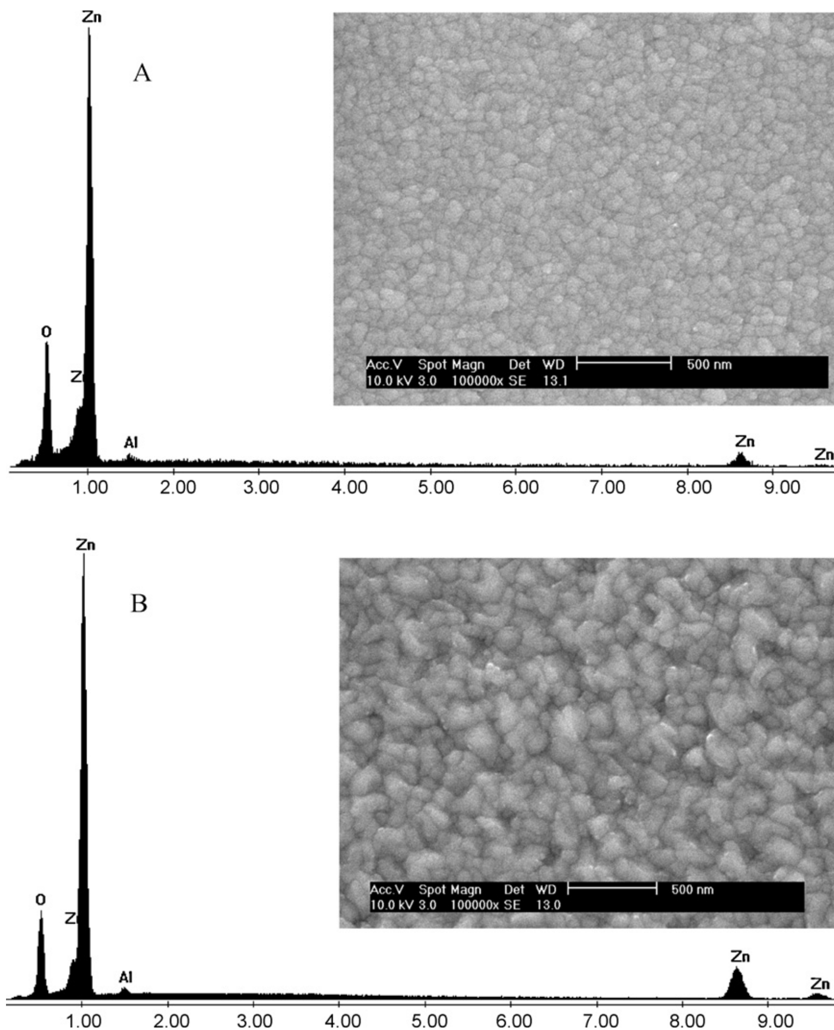

Fig. 5. SEM and EDS images of AZO films before (A) and after (B) annealing at 400 °C.

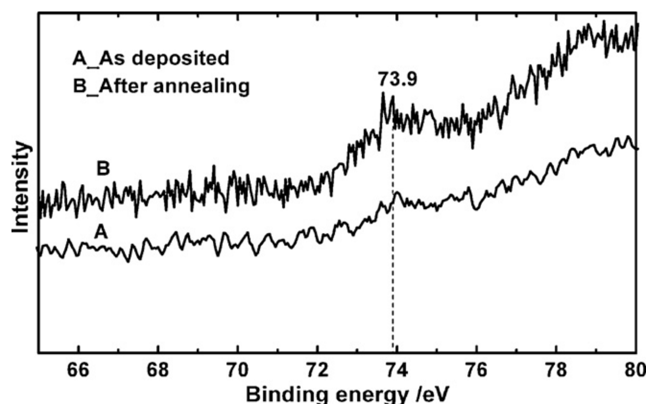

Fig. 6. Al2p spectra of AZO films before and after annealing at 400 °C.

of as-deposited and annealed (400 °C) AZO films are 12.6 nm and 13.9 nm, respectively.

On the contrary, the relative weak peaks like (1 0 1), (1 0 3), (1 1 2), etc. are undesirable for conductivity improvement. Unfortunately, these peaks have also been enhanced during the re-firing process, which always lead to a jumbled structure in which defects such as massive disordered grain boundaries acting as carrier trapping sites always exist. Subsequently, the carrier mobility and concentration decrease as mentioned in Section 3.1. As annealing time increases, these negative factors might overpower the positive ones discussed above, which might then partly explain the increasing R_s during the later period.

As displayed in Fig. 5, crystal grains of AZO film annealed at 400 °C are obviously larger than those of the as-deposited film, which has already been verified by the XRD results. It should be noticed that the grain size shown by the SEM images is apparently larger than that calculated from the XRD results. The reason is that the XRD deduced grain size is the average dimension of the crystallites normal to the reflecting planes, while the grain size derived from the SEM images is the distance between two visible grain boundaries. The discrepancy between these two results could just serve as evidence for the AZO film's uneven growth behavior in different directions under certain conditions. Moreover, as reported [25], a more diverse oriented rough surface can also be noticed in Fig. 5, which was also induced by the ubiquitous grain growth. The compositional results from a larger area, which cover the region yielding the SEM image of the film have been determined by EDS and are displayed in Fig. 5. It indicates that within the sensitivity range of EDS, other than the elements composing AZO films, there are no extra elements, which might affect the film properties before and after the annealing.

3.3. Chemical bonding states

Surface states are believed to be critical for the performances of thin films, and there is no exception for AZO. Thus, chemical binding states of the three AZO composing elements in the film surface have been analyzed with XPS spectra before and after annealing at 400 °C. In the spectra, all peaks have been normalized by binding energy of C1s (284.6 eV). Due to the few doping amounts of Al and its leanness in the surface, there is only weak trace for Al2p in Fig. 6, thus quantitative research on it is unfeasible. For qualitative analysis, the only perceivable peak at 73.9 eV yet corresponds to stoichiometric Al_2O_3 [29–31], which has not been detected by X-ray diffraction due to its meagre concentration. In n-type AZO films, interstitial Al atoms and Al^{3+} ions on the substitutional sites of Zn ions are expected to share the role of electrical carrier donors with oxygen vacancies and interstitial Zn atoms to donate free electrons. In contrast, Al^{3+} ions in Al_2O_3 phase have been confirmed as carrier scattering center and believed to be harmful to the electrical conductivity [24,32]. Therefore, the occurrence and enhance of Al_2O_3 phase evidenced by Fig. 6 can be one of the critical reason for the increase of R_s at higher temperatures as discussed in Fig. 2.

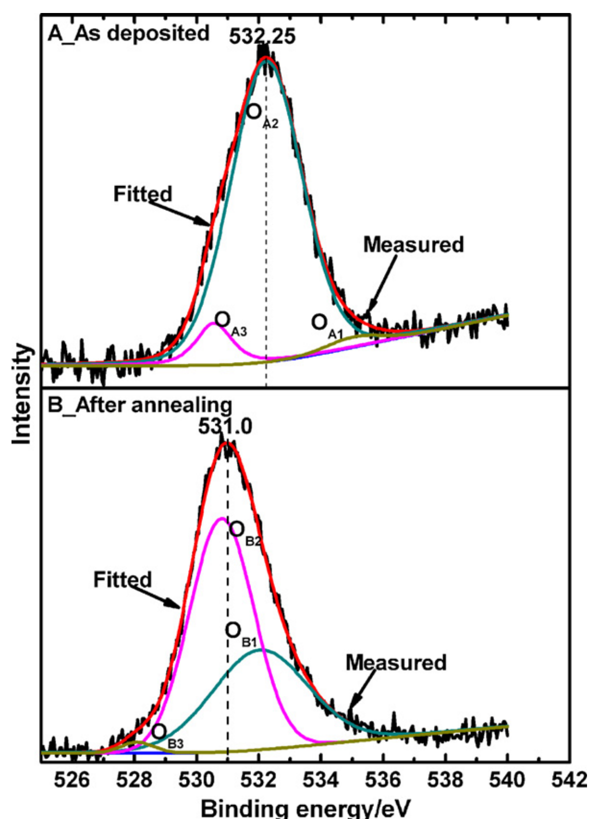

Fig. 7. O1s spectra of AZO films before and after annealing at 400 °C.

As given in Fig. 7(A), the measured O1s peak is centered at 532.25 eV before annealing. The three single gauss-resolved peaks marked as O_{A1}, O_{A2}, and O_{A3} are at 535.05, 532.24 and 530.56 eV, respectively. The highest energy O_{A1} peak can be attributed to weakly bounded oxygen species in the form of $-CO_3$, $-OH$ or adsorbed O_2 [29,33,34]. O_{A2} with medium energy generally belongs to O^{2-} ions in an oxygen deficient matrix. The relative largest O_{A2} area indicates that there are massive oxygen vacancies supplying charge carriers in the film, which is essential for AZO conductivity. O_{A3} with lower binding energy is always attributed to oxygen ions in Zn–O bonds within fully oxidized normal wurtzite matrix [29,35]. After annealing at 400 °C, by comparison with Fig. 7(A), it can be noticed that the measured peak in Fig. 7(B) shifts to a lower energy of 531 eV. On one hand, the high energy peak relating to loosely bonded oxygen vanishes in Fig. 7(B), which demonstrates the chemisorbed oxygen might has been effectively removed or changed to another forms; on the other hand, compared with Fig. 7(A), the ratio of the peak area belonging to O^{2-} ions in oxygen deficient matrix (O_{B1} peak at 532.03 eV) to that belonging to O^{2-} ions in fully oxidized matrix (O_{B2}, O_{B3} at 530.81, and 528.09 eV) has been largely depressed in Fig. 7(B). In other words, after annealing at 400 °C, oxygen vacancies acting as charge carrier donors have been diminished and replaced by fully oxidized species, which might partially derived from the vanished chemisorbed oxygen. In conclusion, state transformations of the oxygen in the surface are

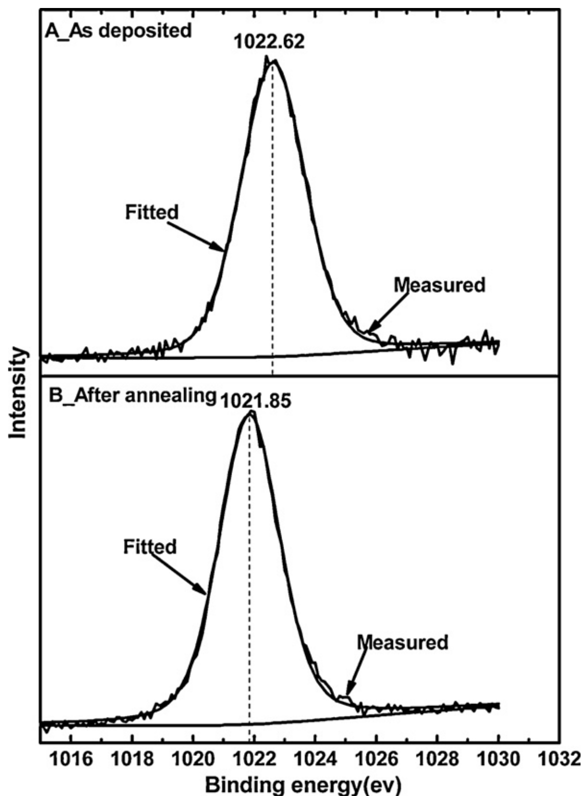

Fig. 8. Zn2p3/2 spectra of AZO films before and after annealing at 400 °C.

undesirable and could be responsible for the increase of R_s in Fig. 2 too.

With respect to Zn2p3/2, which is shown in Fig. 8(A), before annealing, it can be gauss-resolved to only one peak at 1022.62 eV, which just stands for zinc in Zn–O bonds [35,36]. Binding energy of 1021.5 eV was attributed to metallic zinc atoms, which have been reported as difficult to be detected in AZO films [36]. Therefore, though the measured peak remarkably shifts to lower position of 1021.85 eV after annealing as shown in Fig. 8(B), it was still inapplicable to fit Zn2p3/2 spectra to more than one peak with an envisioned peak at 1021.5 eV. This decrease of binding energy has been reported to be the result of that more Zn atoms are bound to oxygen atoms [37], which subsequently implies a decrease of Zn interstitials and then the decay of electrical conductivity in our work.

Based on results from Figs. 7 and 8, the surface atomic ratios (R) Zn/O can be obtained by:

$$R = \frac{A_{Zn}/I_{Zn}}{A_O/I_O} \quad (3)$$

where A is the integral XPS peak area of the corresponding element, and I is the sensitive indexes ($I_{Zn2p3/2} = 4.24$, $I_{O1s} = 0.61$). The calculated Zn/O ratios for the original and annealed AZO films are 0.43 and 0.58, separately, which implies that the surface of the room temperature sputtered film is highly oxygen enriched. Furthermore, give this increased surface Zn/O ratio and the above discussions into consideration, we highly suggest that certain out-diffusion of Zn atoms even Al atoms toward the film surface, and in-diffusion of loose bounded oxygen atoms toward the film body have occurred during the higher temperature annealing. We also propose that certain chemical reactions have also happened during such process, which has already been confirmed by Yun et al. [31] in AZO films irradiated by high-energy electron beam. Eventually, these arguments can again help us to further explain the chemical state transformations for the three elements accordingly, and then the variations of electrical properties.

4. Conclusions

When AZO films were heated at temperatures over 100 °C, their sheet resistance behaved differently at different stage. The sheet resistance decreased at early stage but increased then to the end. Higher temperatures always resulted in higher sheet resistance eventually. Certain possible phase transitions may also take place during the higher temperature annealing. EDS results indicated that besides zinc, aluminum and oxygen in the films, there had no extra element, which can influence the films' electrical properties before and after the annealing. Analysis implied that growth of *c*-axis oriented ZnO grains and the release of residual stress during the annealing are beneficial for the film conductivity, yet the growth of non *c*-axis oriented grains and non ZnO phases like Al_2O_3 are harmful which might dominant later. The remarkable high oxygen concentration in the film surface could be responsible for the instability of the film conductivity. Further investigations are necessary to confirm and improve thermal stability of AZO films for high temperature applications.

References

[1] W.W. Zhong, F.M. Liu, L.G. Cai, C.C. Zhou, P. Ding, H. Zhang, J. Alloys Compd. 499 (2010) 265–268.
[2] M. Benhaliliba, C.E. Benouis, M.S. Aida, A. Sanchez Juarez, F. Yakuphanoglu, A. Tiburcio Silver, J. Alloys Compd. 506 (2010) 548–553.
[3] H.X. Liu, B.B. Huang, Z.Y. Wang, X.Y. Qin, X.Y. Zhang, J.Y. Wei, Y. Dai, P. Wang, M.H. Whangbo, J. Alloys Compd. 507 (2010) 326–330.
[4] Y.X. Liu, H.L. Zhang, X.Y. An, C.T. Gao, Z.X. Zhang, J.Y. Zhou, M. Zhou, E.Q. Xie, J. Alloys Compd. 506 (2010) 772–776.
[5] B. Wang, L.D. Tang, J.G. Qi, H.L. Du, Z.B. Zhang, J. Alloys Compd. 503 (2010) 436–438.
[6] C. Xu, L.X. Cao, G. Su, W. Liu, X.F. Qu, Y.Q. Yu, J. Alloys Compd. 497 (2010) 373–376.
[7] J.X. Mou, W.G. Zhang, J. Fan, H. Deng, W. Chen, J. Alloys Compd. 509 (2011) 961–965.
[8] X.Y. Xu, C.B. Cao, J. Alloys Compd. 501 (2010) 265–326.
[9] Z.L. Lu, X.F. Bian, W.Q. Zou, M.X. Xu, F.M. Zhang, J. Alloys Compd. 492 (2010) 31–34.
[10] T. Prasada Rao, M.C. Santhosh Kumar, J. Alloys Compd. 506 (2010) 788–793.
[11] Z. Lockman, Y.P. Fong, T.W. Kian, K. Ibrahim, K.A. Razak, J. Alloys Compd. 493 (2010) 699–706.
[12] P.G. Li, Q.R. Hu, W.H. Tang, J. Alloys Compd. 509 (2011) 2776–2779.
[13] S. Cornelius, M. Vinnichenko, N. Shevchenko, A. Rogozin, A. Kolitsch, W. Moller, Appl. Phys. Lett. 94 (2009) 042103.
[14] C.P. Liu, G.R. Jeng, J. Alloys Compd. 468 (2009) 343–349.
[15] E.J. Yun, J.W. Jung, B.C. Lee, J. Alloys Compd. 496 (2010) 543–547.
[16] O. Hamad, G. Braunstein, H. Patil, N. Dhere, Thin Solid Films 489 (2005) 303.
[17] A. El Manouni, F.J. Manjon, M. Perales, M. Mollar, B. Mari, M.C. Lopez, J.R. Ramos Barrado, Superlattices Microstruct. 42 (2007) 134.
[18] T. Minami, T. Miyata, T. Yamamoto, J. Vac. Sci. Technol. A 17 (1999) 1822.
[19] T. Tsuji, M. Hirohashi, Appl. Surf. Sci. 157 (2000) 47.
[20] X. Chen, W. Guan, G. Fang, X.Z. Zhao, Appl. Surf. Sci. 252 (2005) 1561.
[21] B.Y. Oh, M.C. Jeong, D.S. Kim, W. Lee, J.M. Myoung, J. Cryst. Growth 281 (2005) 475.
[22] Z.L. Yuan, X.T. Zu, S.W. Xue, X.P. Li, X. Xiang, B.Y. Wang, D.B. Tian, H. Deng, F.Y. Mao, Semicond. Optoelectron. 29 (2008) 548.
[23] G.J. Fang, D. Li, B.L. Yao, Thin Solid Films 418 (2002) 156–162.
[24] W.F. Yang, Z.Y. Wu, Z.G. Liu, A.S. Pang, Y.L. Tu, Z.C. Feng, Thin Solid Films 519 (2010) 31–36.
[25] H.J. Ch, S.U. Lee, B. Hong, Y.D. Shin, J.Y. Ju, H.D. Kim, M. Park, W.S. Choi, Thin Solid Films 518 (2010) 2941–2944.
[26] H.C. Cheng, C.F. Chen, C.Y. Tsay, J.P. Leu, J. Alloys Compd. 475 (2009) L46–L49.
[27] Y.F. Gu, X.M. Li, W.D. Yu, X.D. Gao, J.L. Zhao, C. Yang, J. Cryst. Growth 305 (2007) 36–39.
[28] H. Kaga, Y. Kinemuchi, S. Tanaka, A. Makiya, Z. Kato, K. Uematsu1, K. Watari, Jpn. J. Appl. Phys. 45 (2006) L1212–L1214.
[29] Y.M. Chung, C.S. Moon, M.J. Jung, J.G. Han, Surf. Coat. Technol. 200 (2005) 936.
[30] NIST XPS Database, Selected Element Search Result, http://srdata.nist.gov/xps.
[31] E.-J. Yun, J.W. Jung, K.N. Ko, J. Hwang, B.C. Lee, M.-H. Jung, Thin Solid Films 518 (2010) 6236–6240.
[32] K. Ellmer, F. Kudella, R. Mientus, R. Schieck, S. Fiechter, Thin Solid Films 247 (1994) 15.

[33] T. Szorenyi, L.D. Laude, I. Bertoti, Z. Kantor, Z. Geretovszky, J. Appl. Phys. 78 (1995) 6211.
[34] D.K. Kim, H.B. Kim, J. Alloys Compd. 509 (2011) 421–425.
[35] M.N. Islam, T.B. Ghosh, K.L. Chopra, H.N. Acharya, Thin Solid Films 280 (1996) 20.
[36] M. Chen, X. Wang, Y.H. Yu, Z.L. Pei, X.D. Bai, C. Sun, R.F. Huang, L.S. Wen, Appl. Surf. Sci. 158 (2000) 134.
[37] M. Tanemura, H. Hatano, M. Kudo, N. Ide, Y. Fujimoto, L. Miao, H.Y. Yang, S.P. Lau, S.F. Yu, J. Kato, Surf. Sci. 601 (2007) 4459.